JOURNAL OF MATERIALS SCIENCE 12 (1977) 97–116

Dynamic solid particle damage in brittle materials: an appraisal

A. G. EVANS
Science Center, Rockwell International, Thousand Oaks, California, USA

T. R. WILSHAW
Effects Technology, Inc, Santa Barbara, California, USA

The damage caused by solid projectiles in the elastic and elastic/plastic target response regimes has been characterized and analysed. Semi-empirical methods for establishing the relative importance of the target and properties on the impact damage have been derived, based on quasi-static indentation fracture characterization schemes and the quantification of the impact damage observations.

1. Introduction

The damage created on brittle surfaces by quasi-static solid particle contact has been extensively studied in both the elastic [1] and elastic/plastic [1, 2] indentation regimes. In the elastic regime, the maximum tensile stresses are radial, creating circumferential cracks which initiate at the surface and propagate inward. In the elastic/plastic regime the maximum tensile stresses near the surface are tangental and produce radial cracks which propagate outwards along the surface; while, in the sub-surface, the maximum tensile stresses are approximately parallel to the surface, and create sub-surface lateral cracks. The formation of the circumferential cracks is determined by (a) the flaw properties of the test material as determined by the fracture toughness, K_C, and the surface flaw size distribution, $\Phi(a)$, and (b) the stress field parameters as determined by the elastic properties of the material and the indenter and the indenter geometry. Flaw formation, which is thus a strong function of the surface state of the material (except when the flaws are relatively large), has been widely studied and shown to be amenable to characterization by quasi-static indentation tests and by applying flaw statistics. The extension of the circumferential cracks, which is determined by K_C and the stress field parameters, has also been extensively studied and is now reasonably well understood. The formation condition for the radial and lateral cracks has not been clearly defined, although approximate formation criteria have been suggested [2]. However, their extension has been fully characterized [3] in terms of the hardness, H, the toughness K_c, and the elastic modulus, E, of the test material, as shown for the radial cracks in Fig. 1.

The quasi-static indentation characteristics have been utilized to evaluate such important phenomena as abrasive wear [2, 4] and low velocity erosion [2]. However, the equally important dynamic erosion phenomenon cannot be regarded as a simple extension of the quasi-static process, because substantial changes in material response may accompany the dynamic loading. The dynamic properties that relate to projectile impact are not well understood, and it is the objective of the present study to suggest semi-empirical approaches for characterizing dynamic solid particle damage in brittle materials, as a basis for identifying the material parameters that exert the prime influence on dynamic erosion.

A survey of the available impact theory, as it might pertain to projectile impact, is presented in the first section in order to provide a rationale for the impact experiments and analyses. Impact experiments which induce both elastic and elastic/plastic target response are then conducted, and the impact damage in both regimes is quantified. Quasi-static indentation experiments (which establish the elastic flaw formation properties and the plastic response of the target material)

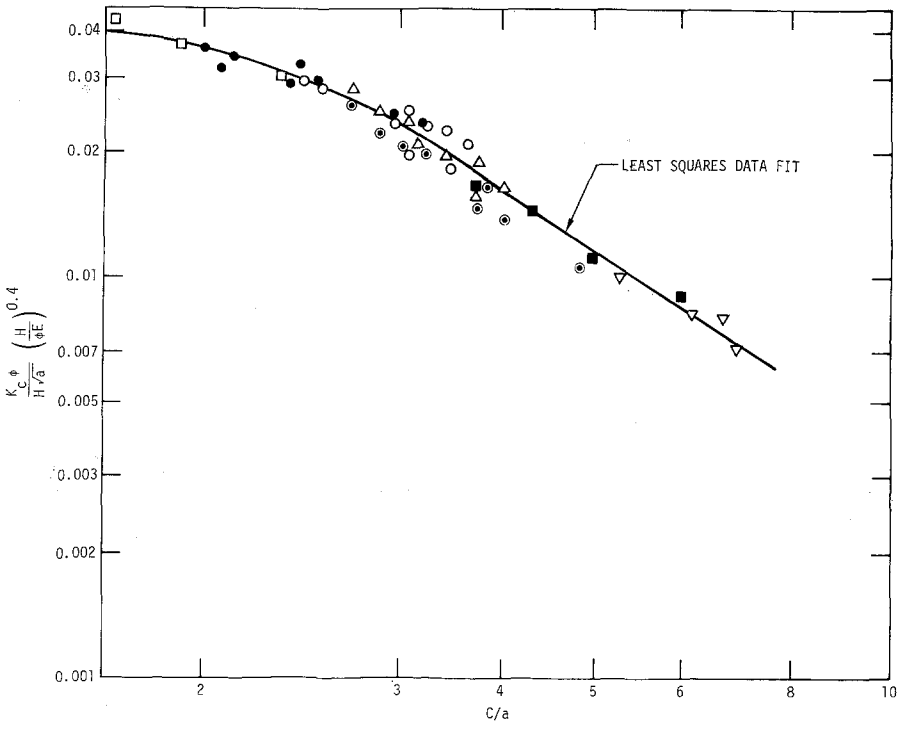

Figure 1 A characterization of the radial fracture obtained for quasi-static indentation in the elastic/plastic regime [3].

are also performed to provide some of the target characteristics required for damage analysis. Finally, the impact damage is analysed, using a combination of the quasi-static fracture characterization and simple impact theory.

2. Impact theory

2.1. Contact characteristics

The contact between the projectile and the target is of prime importance in determining the mode and the extent of the damage caused by particle impact. The crucial contact parameters are the pressure, p, the contact radius, a, and the contact time, t. The pressure, which essentially determines whether the target response will be elastic or plastic, is of primary initial concern. Then, the contact radius relates the pressure to the effective applied force, P ($p \approx P/\pi a^2$), and the contact time determines the force history, P (t). This force history ultimately establishes the extent of the impact damage, for a specified contact condition, because it directly determines the magnitude of the dynamic stresses outside the contact zone. Two approaches have been used to relate the force history to the target and projectile properties; a quasi-static method and a one-dimensional dynamic method. These approaches are described below and then an approximate method for predicting the response of the target (elastic or plastic) is presented.

2.1.1. Quasi-static analysis

The quasi-static approach involves the solution of the laws of motion which relate the penetration to the projectile momentum. This type of analysis yields the following relations [2, 5]:

$$P_{\max} = (E_t b^2) f_1\left(\frac{v_0 \rho_p}{E_t}\right) f_2\left(\frac{p}{E_t}\right)$$

$$t_{\max} = \left(\frac{R}{v_0}\right) f_3\left(\frac{v_0 \rho_p}{E_t}\right) f_4\left(\frac{E_t}{p}\right) \qquad (1)$$

where E is Young's modulus, b is the projectile radius, ρ is the density, v_0 is the initial velocity, f_{1-4} are functions which depend on the penetration function $P(z)$, and the subsceipts p and t refer respectively to the projectile and the target. The force histories for elastic contact, or for a constant plastic contact pressure (or equivalently, a constant dynamic hardness, H_d), are shown schematically in Fig. 2a. For a target with a more typical rate-dependent plastic response (whereupon the dynamic hardness is an increasing function of the displacement rate, $\dot{z}$) the force

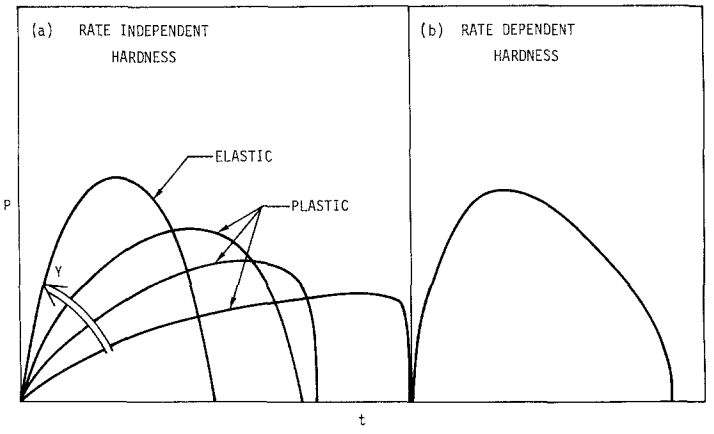

Figure 2 A schematic illustration of the force history expected from projectile impact for (a) elastic and rate-independent plastic contact (Y signifies yield strength), (b) ratedependent plastic contact.

history in the plastic regime exhibits the characteristics depicted in Fig. 2b. Hence, whenever quasi-static contact conditions prevail, the important contact parameters can be expressed in terms of the target and projectile parameters (p, E_t, b, v_0, ρ_p), if the pertinent $P(z)$ is known. For elastic contact $P(z)$ is given by the Hertz analysis [1]; however, for elastic/plastic contact, or for target densification, $P(z)$ is less well characterized [2, 5], and the function $P(\dot{z})$ is generally unknown in the appropriate range of $\dot{z}$.

2.1.2. Dynamic analysis

The transient contact between impacting bodies is characterized by the relations between the particle velocity, u_p, the pressure p and the wave velocity, u_s as derived from shock wave studies. The important relations for a one-dimensional contact are:

$$u_s = c_1 + S\Delta u_p$$
$$p = \rho u_p \qquad (2)$$

where c_1 is the longitudinal elastic wave velocity, S is an experimentally determined material constant ($0 < S < 2$) and Δu_p is the discontinuity in particle velocity. Combining these equations to eliminate u_s, gives:

$$p = \rho c_1 \Delta u_p + \rho S(\Delta u_p)^2. \qquad (3)$$

Typical pressure–particle velocity curves for materials of interest in the present study are presented in Fig. 3. These curves can be used directly to provide an estimate of p and u_i for initial contact, i.e. while the first shock wave is traversing the projectile. This estimate neglects elastic constraint effects which might occur in three-dimensional projectile impact problems*, and the result should only be regarded as a preliminary estimate. At initial contact, the target is at rest and the projectile is moving with a velocity v_0 (Fig. 1a). Hence, essentially instantaneous changes in the target/projectile particle velocities must occur along the contact surface, to achieve a mutually compatible particle velocity, u_i, at the interface. This particle velocity, if assumed to be constant, can be found to a good approximation from Equation 3 by equating p_p and p_t to obtain;

$$u_i^2(\rho_t S_t - \rho_p S_p) + u_i(\rho_t c_t + \rho_p c_p + 2\rho_p S_p v_0) - \rho_p v_0(c_p + S_p v_0) = 0. \qquad (4)$$

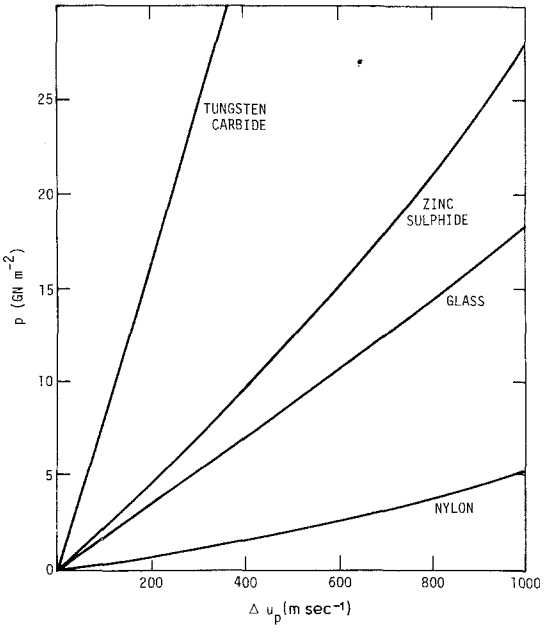

Figure 3 Pressure, particle velocity curves for the materials used in this study.

* In the quasi-static case this effect accounts for a factor of 3 in the contact pressure [2].

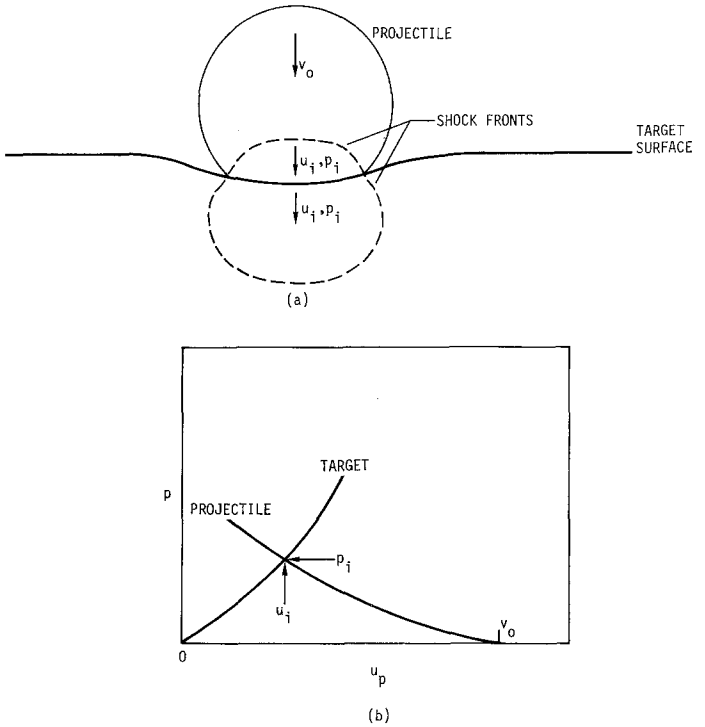

Figure 4(a) A schematic illustration of the contact between a spherical projectile and a planar surface indicating the approximate form of the pressure and particle velocity distribution. (b) A schematic illustration of the intersection method for estimating the contact pressure and particle velocity.

A convenient graphical solution to Equation 4 plots the target pressure curve from a zero velocity origin, and the inverted projectile curve from a v_0 origin (Fig. 4) to obtain the intercept velocity. This velocity can then be equated directly to the average interface velocity, u_i, while the intercept pressure yields the corresponding average interface pressure, p_i. When the shock wave in the projectile reflects from the rear surface and arrives back at the interface there will be another discontinuity in particle velocity, and a corresponding drop in the pressure p_i. This is, however, a complex process in spherical or irregularly shaped projectiles (because of interactions between the reflected and incident waves) which has not yet been adequately modelled.

The other contact parameter required to characterize the contact is the contact radius, $a(t)$. For incompressible projectiles this is simply obtained from the projectile profile. For spherical projectiles:

$$a = \sqrt{[(2b - u_i t)u_i t]} \tag{5}$$

which, for $a \ll b$, reduces to:

$$a \approx \sqrt{(2bu_i t)}. \tag{6}$$

The force history for initial contact thus given by:

$$P = p_i \pi u_i t(2b - u_i t). \tag{7}$$

These relations are expected to be reasonably valid when $E_p \gg E_t$ and hence, usually, when $\rho_p c_p \gg \rho_t c_t$. The corresponding relations for compressible projectiles are not known.

2.1.3. Target response

The shock wave properties of the target in the non-linear region (Fig. 5) should provide an estimate (see above) of the plastic response of the target to indentation at a velocity u_p, and can thus be regarded as a measure of the dynamic hardness of the material at large particle velocities (or displacement rates). If the pressure exhibits a discontinuity where it first deviates from linearity (the equivalent of a dynamic yield condition), this discontinuity is an approximate indication of the onset of plastic deformation in the target. Alternatively, direct hardness measurements provide dynamic hardness properties at much lower displacements rates (Fig. 5). In this regime, H_d is usually a function of $\dot{z}$ at small $\dot{z}$, because the deformation is thermally activated [6], while at larger $\dot{z}$, where the deformation (at least in

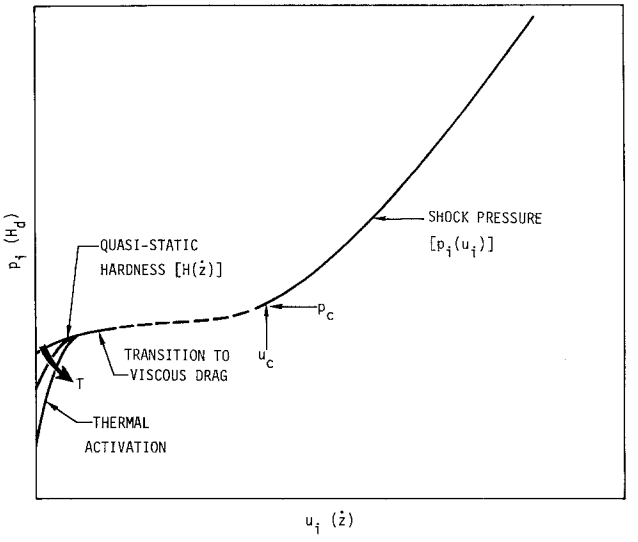

Figure 5 The combination of one-dimensional shockwave and quasi-static hardness data to produce a "dynamic hardness" curve; T indicates temperature.

crystalline materials) approaches the viscous drag regime, H_d becomes less sensitive to $\dot{z}$.

An extrapolation of the latter region to intersect the shock wave curve might thus define an approximate particle velocity, u_c, and pressure, p_c, at which the target begins to respond plastically. For a specified target/projectile combination there will thus be a critical projectile velocity, v_c,* above which the target should deform plastically; this velocity should increase as $\rho_p c_p$ decreases.

2.2. Dynamic stress fracture analysis

For elastic target response, the amplitude and duration of the transient elastic stresses have been estimated analytically by Blowers [7]. The important target parameters involved in impact damage can be obtained directly from the normalized stress wave parameters used by Blowers (even though the restricted assumptions about the contact parameters used to obtain an analytic solution may limit the quantitative utility of the analysis). The normalized parameters are:

$$\Omega = \sigma/p_i$$
$$R = 4c_t r/k^2$$
$$T = 4c_t^2 t/k^2 \qquad (8)$$

where σ is the stress amplitude, r is the distance from the centre of contact, t is the time after initial contact and k is a quantity determined by the contact parameters. Typical values of the radial stress Ω_r as a function of time T, obtained $\sim 5\,\mu$m below the target surface [8] are plotted in Fig. 6 for several distances R from the contact centre.

The importance of this plot can be appreciated when crack formation and crack arrest conditions are superimposed. For elastic contact, since the radial near-surface tensile stresses initiate fracture [1], the average crack formation stress, $\bar{\sigma}_c$ (obtained by quasi-static indentation [1]), can be converted into the corresponding normalized stress $\bar{\Omega}_c$ (σ_c/p_i), and superimposed on Fig. 6 to show that there should be a zone of fracture initiation, ΔR, which increases as ($p_i/\bar{\sigma}_c$) increases. Further, since from Equation 8,

$$\Delta r = \frac{k^2 \Delta R}{4c_t} \qquad (9)$$

the absolute extension of this zone, Δr, should diminish as the wave velocity in the target increases.

Crack arrest is a substantially more complex process to characterize than crack formation, but the essence of the problem is contained in the approximate description presented in the Appendix. The principal result is that the crack arrest length, C_a, should be related to the important target and projectile properties by the following approximate proportionality:

$$C_a \propto \frac{k^2}{c_t} \Delta T(p_i/K_c \cdot p_i/\bar{\sigma}_c) \qquad (10)$$

where K_c is the fracture toughness of the target.

* The critical velocity is probably also a function of the projectile radius, which should influence u_i when the three-dimensional asepcts of the contact are introduced.

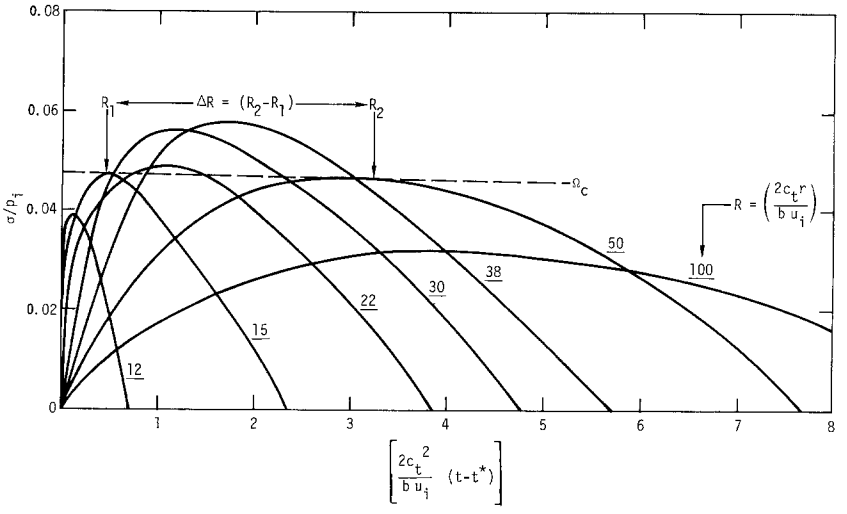

Figure 6 Approximate tensile stress versus time curves at constant position, plotted using Blower's normalized coordinates, as derived from Adler's numerical data [8] (obtained at ~ 5 μm below the surface). Small, localized stress peaks have been omitted and some interpolation has been used for simplicity of presentation. t^* is the time when the stresses at each position first become tensile.

The damage zone and the crack extension that result from transient *elastic* stresses should thus depend inversely on the longitudinal wave speed in the target*, the flaw formation stress (or equivalently, the size distribution of pre-existing flaws in the vicinity of the surface) and the fracture toughness. The contact parameters, notably the interface pressure and particle velocity, (the latter via the k term in Equations 9 and 10) should also affect the damage. However, changes in the target properties which reduce u_i, must increase p_i (see Fig. 4b), and since these contact parameters enter the damage relations through some product of p_i and u_i, the effect on the damage depends on the relative changes in u_i and p_i. Qualitatively we note that for small $\rho_p c_p$ the relatively larger reduction in u_i achieved by increasing $\rho_t c_t$ is likely to be dominant, reinforcing the beneficial effect of c_t on damage reduction; while, for large $\rho_p c_p$, the increase in p_i may be dominant, partly negating the beneficial effect of c_t.

For plastic target response there are no equivalent analytic solutions which could provide a similar rationale for damage characterization.

2.3. Appraisal

The simplified impact theories presented above are clearly limited in scope. However, complete three-dimensional analyses of projectile impact, which are complex numerical problems, contain several unknowns and such analyses (although useful) are often found to have restricted utility. An alternative approach is to use the simplified theories, in conjunction with empirical impact damage observations to provide a semi-empirical framework for the prediction of impact damage. This semi-empirical approach to the impact problem uses the one-dimensional shock wave analysis or the quasi-static analysis (with a rate-independent quasi-static hardness) to estimate the contact parameters. Then, the normalized fracture parameters obtained by quasi-static indentation, modified (if necessary) by the dynamic stress field parameters, are used as a basis for an iterative correlation of the observed impact damage with the contact parameters.

3. Experimental

3.1. Impact studies

3.1.1. Materials selection

A single target material which is isotropic and well-characterized, and exhibits both elastic and plastic contact behaviour with readily available projectile materials, would be appropriate for this study. Optical transparency would also be a major advan-

* This may account for the approximate inverse correlation of the raindrop damage in brittle materials with the target hardness [9], because the hardness in such materials tends to scale with the elastic modulus [2] and hence, with the wave velocity.

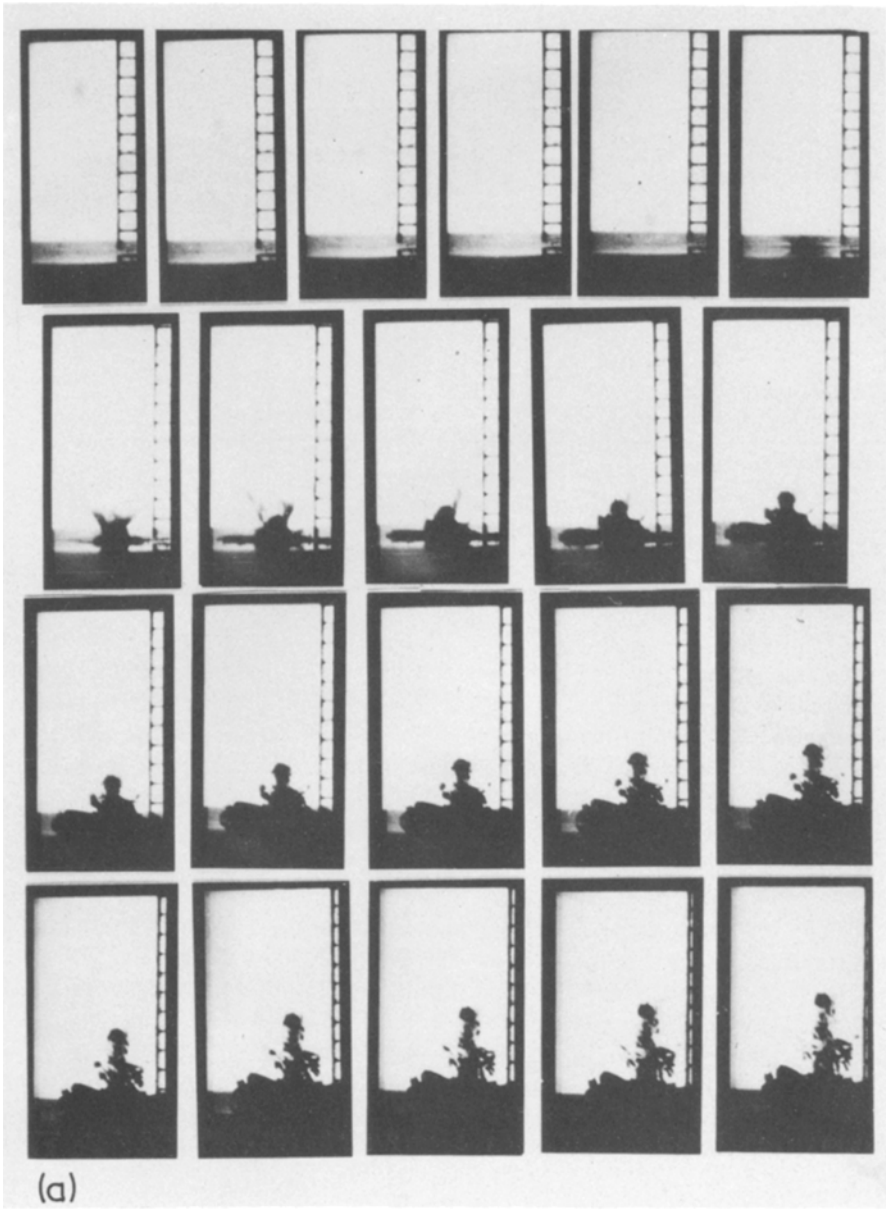

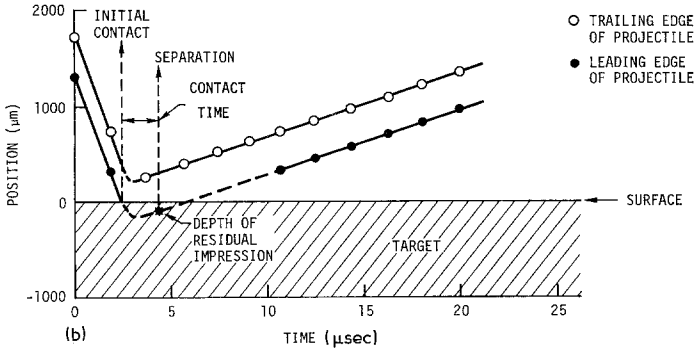

Figure 7(a) A photographic sequence showing a 400 μm WC projectile impinging on a ZnS target at 520 m sec^{-1}; note the target ejecta (grid 500 μm, time between frames 1.74 μsec). (b) A penetration curve developed from (a), indicating the expected contact time.

TABLE I Summary of impact test results

Projectile	Velocity ($m\,sec^{-1}$)	Mass loss ratio	Contact time (μsec)	Impulse ($m\,kg^{-1}\,sec^{-1}$)	
				Direct	Indirect
	130*	0.018			
WC	230*	0.38		1.55×10^{-4}	1.6×10^{-4}
(400 μm)	520*	4.92	2.2	4.2×10^{-6}	4.1×10^{-4}
diameter	860*	6.87			
Nylon	1000*	0	<0.2		
(500 μm	633	0	9.0		
diameter)	406	0	5.1		
	302	0			
Glass	160	0			
(1000 μm	350*	0	>1.0	4.5×10^{-4}	
diameter)					

* Average values for three tests are indicated

tage [2]. A material which matches these requirements is chemically vapour-deposited ZnS*, and this material will be used exclusively in the present study.

Shock wave and quasi-static hardness data (see Section 3.2.2) indicate that (a) WC projectiles have a sufficiently large impedance that plastic flow should be induced in the ZnS targets for all velocities exceeding $\sim 150\,m\,sec^{-1}$, (b) nylon projectiles have a sufficiently low impedance that a purely elastic target response should occur below $\sim 1000\,m\,sec^{-1}$, (c) glass projectiles have an impedance comparable to ZnS and should produce a transition from elastic to plastic response in the target materials within the velocity range, 100 to $1000\,m\,sec^{-1}$. Hence, WC, nylon and glass projectiles, 400 to 1000 μm diameter, have been selected to study damage in the plastic, elastic and transition regimes, respectively.

3.1.2. Test procedures

The high speed projectile impacts were performed using an exploding foil technique [10]. A high speed framing camera was used, in some instances, to record the projectile location immediately prior to, during, and immediately after the contact; and, in other instances, the target was attached to a ballistic pendulum to determine the delivered impulse [11]. The targets and projectiles were carefully weighed before and after contact to determine the mass loss ratio (the ratio of the mass lost from the target to the projectile mass). The target damage after impact was characterized using optical or scanning electron microscopy.

3.1.3. Test results

The impact parameters obtained for each test condition are summarized in Table I. The WC projectiles always remained intact throughout the contact and did not exhibit permanent deformation; the contact times could then be closely estimated from the projectile locations (obtained photographically) and the residual impression depth, as illustrated in Fig. 7. These contact times are included in Table I. The nylon particles exhibited lateral jetting at the higher velocities (Fig. 8), and the contact times (prior to jetting) were too small to be measured with the available camera speeds; upper limits for the contact time, obtained as illustrated in Fig. 8, are thus included in Table I. At the lower velocities the nylon projectiles deformed but did not jet and accurate contact times could then be deduced from the photographic record. The glass projectiles did not deform plastically, but they usually fragmented during the contact (Fig. 9), and the contact time could not easily be deduced from the time dependence of the projectile location (Fig. 9). Thus, fragmentation times after initial contact, which represent a lower limit for the total contact time, are listed in Table I.

3.1.4. Damage observations

The contact in the ZnS caused by the high impedance WC projectiles is plastic over the complete range of test velocities. The damage is almost identical in form to that observed quasi-statically in the plastic regime, with the radial, lateral and median cracks all being evident (Fig. 10a, b and c).

* This is an infra-red window material prepared by the Raytheon Company.

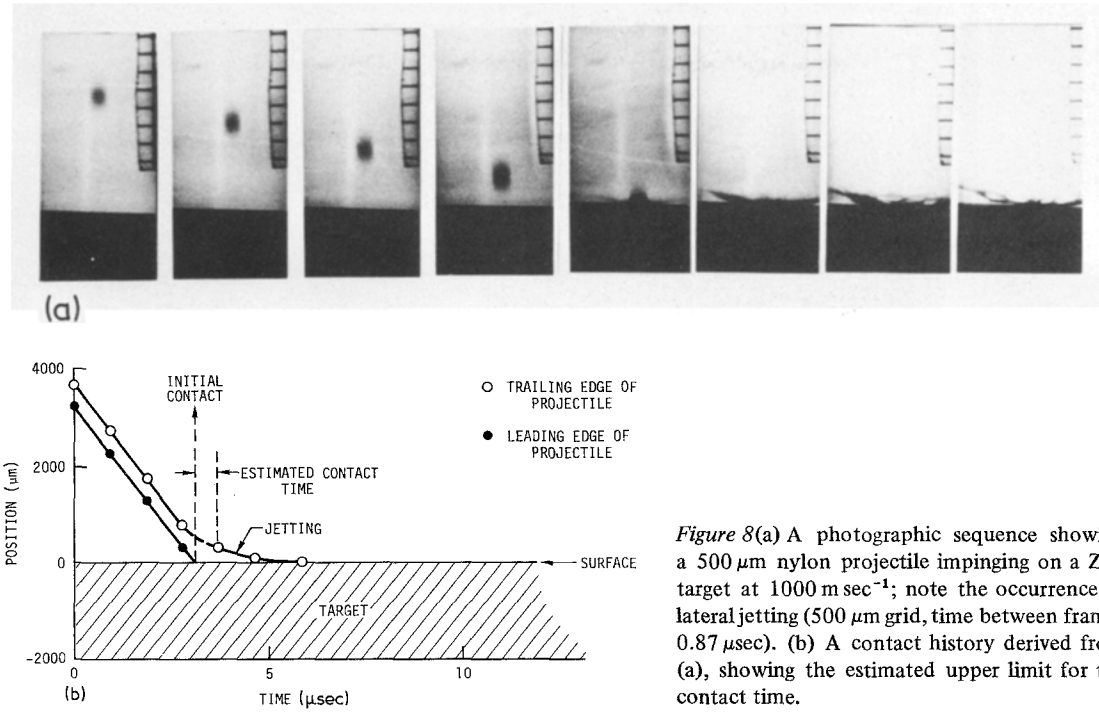

Figure 8(a) A photographic sequence showing a 500 μm nylon projectile impinging on a ZnS target at 1000 m sec^{-1}; note the occurrence of lateral jetting (500 μm grid, time between frames 0.87 μsec). (b) A contact history derived from (a), showing the estimated upper limit for the contact time.

At velocities below $\sim 520\,\mathrm{m\,sec^{-1}}$ the plastic impression remains intact (Fig. 10a), and precise measurements of the maximum contact radius, a, can be made. At large velocities the contact region is partially or wholly removed (Fig. 10d), but it is still possible to estimate the contact radius from the morphology of the central zone. A ridge is formed where the lateral cracks intersect the surface at their inner edge (AB in Fig. 10a). Hence, by measuring the diameter of this ridge (see Fig. 10d) an approximate value for the contact radius is obtained.

Crack length data for radial C_r and lateral C_l cracks obtained in accord with the scheme devised for quasi-static indentation [2] (wherein the crack lengths from the impression centre were related to the contact radius), are plotted in Fig. 11. Also plotted are the corresponding crack lengths obtained quasi-statically, with spheres of identical diameters. It is apparent that the dynamic cracks are several times larger than the quasi-static cracks for the equivalent contact radius, and the divergence increases as the impression radius, or projectile velocity, increase.

The low impedance, nylon projectiles produce damage that is similar in appearance to the damage created by water drops, consisting of a series of approximately concentric circular crack segments within a damage annulus (Fig. 12a). Careful inspection of the central contact region, using high resolution transmission optical microscopy, interference microscopy and cathodoluminescence, indicates that this region contains no resolvable damage (i.e. no defects $> 0.1\,\mu$m in length), has no detectable distortion, and has a low dislocation density. The contact response of the target can thus be regarded as entirely elastic. Observation of the sub-surface damage, using reflected polarized light, shows that there is an inner annulus within the damage zone wherein the sub-surface cracks are approximately paralleled to surface, as exemplified by the region of intense reflection in Fig. 12b; while the cracks in the outer annulus are inclined to the surface, at $\sim 50°$. These features are summarized by the schematic in Fig. 13. The average surface length $\bar{C}_a$ of the segmental cracks in the damage annulus is plotted as a function of the distance, r, from the centre of the contact zone in Fig. 14a, and the average separation, $\overline{\Delta r}$, is plotted in Fig. 14b. The large peak in C_a coincides with a region where two (or more) individual cracks have interacted, such as at A in Fig. 12b. The damage zone increases in extent, and the individual crack lengths increase, as the projectile velocity increases.

The damage caused by the glass projectiles resembles that created at low velocity by the WC projectiles, exhibiting a central plastic impression,

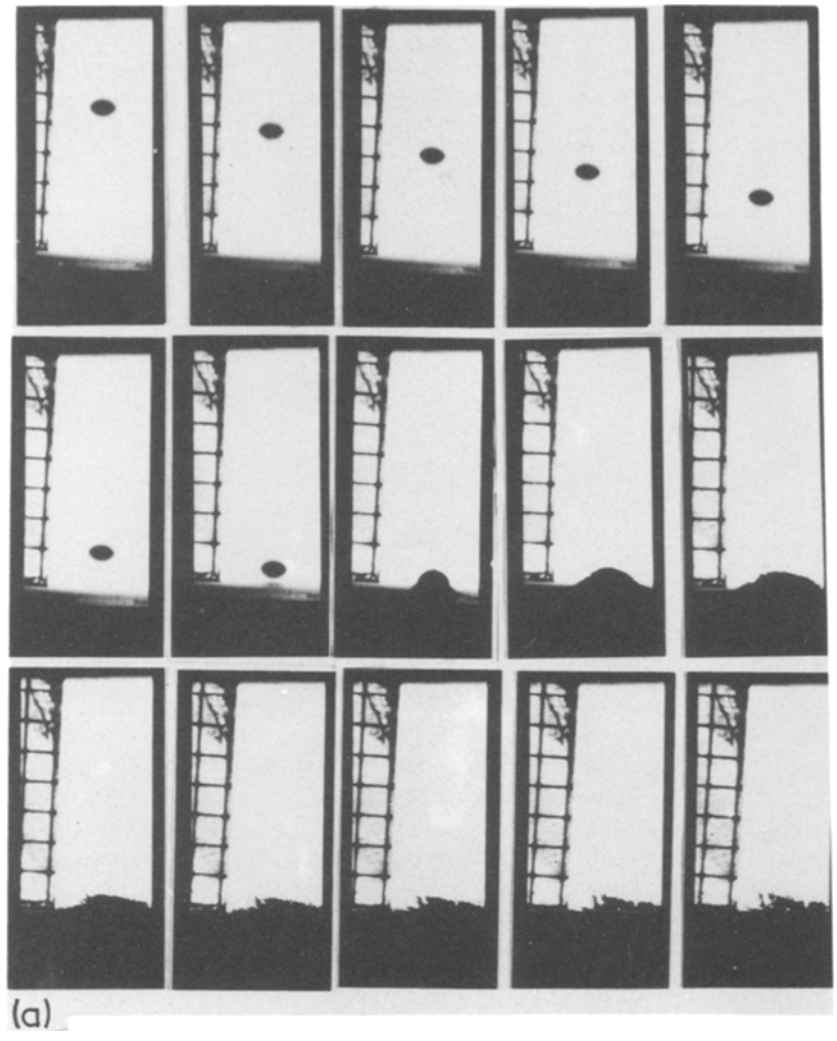

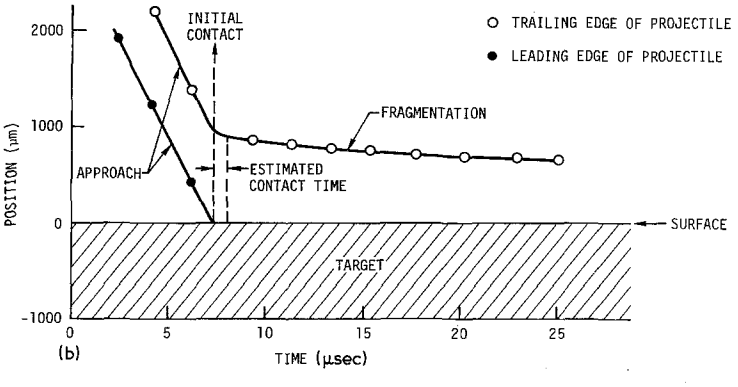

Figure 9 (a) photographic sequence showing a 1000 μm glass projectile impinging on a ZnS target at 350 m sec^{-1}, note the projectile fragmentation (500 μm grid, time between frames 2.17 μsec). (b) A contact history derived from (a), showing the estimated lower limit for the contact time.

as well as radial, lateral and median cracks (Fig. 15a). An additional feature, however, is the occurrence, at the higher projectile velocity, of small areas of material removal within the damage zone (Fig. 15a); this is undoubtedly chipping caused by the small angular glass particles ejected towards the target after fragmentation. Further inspection of the damage at the lower velocity also revealed the presence, outside the central damage zone, of segmental cracks (Fig. 15b), that resemble the cracks formed by the nylon projectiles. Their presence is suggestive of an imminent transition

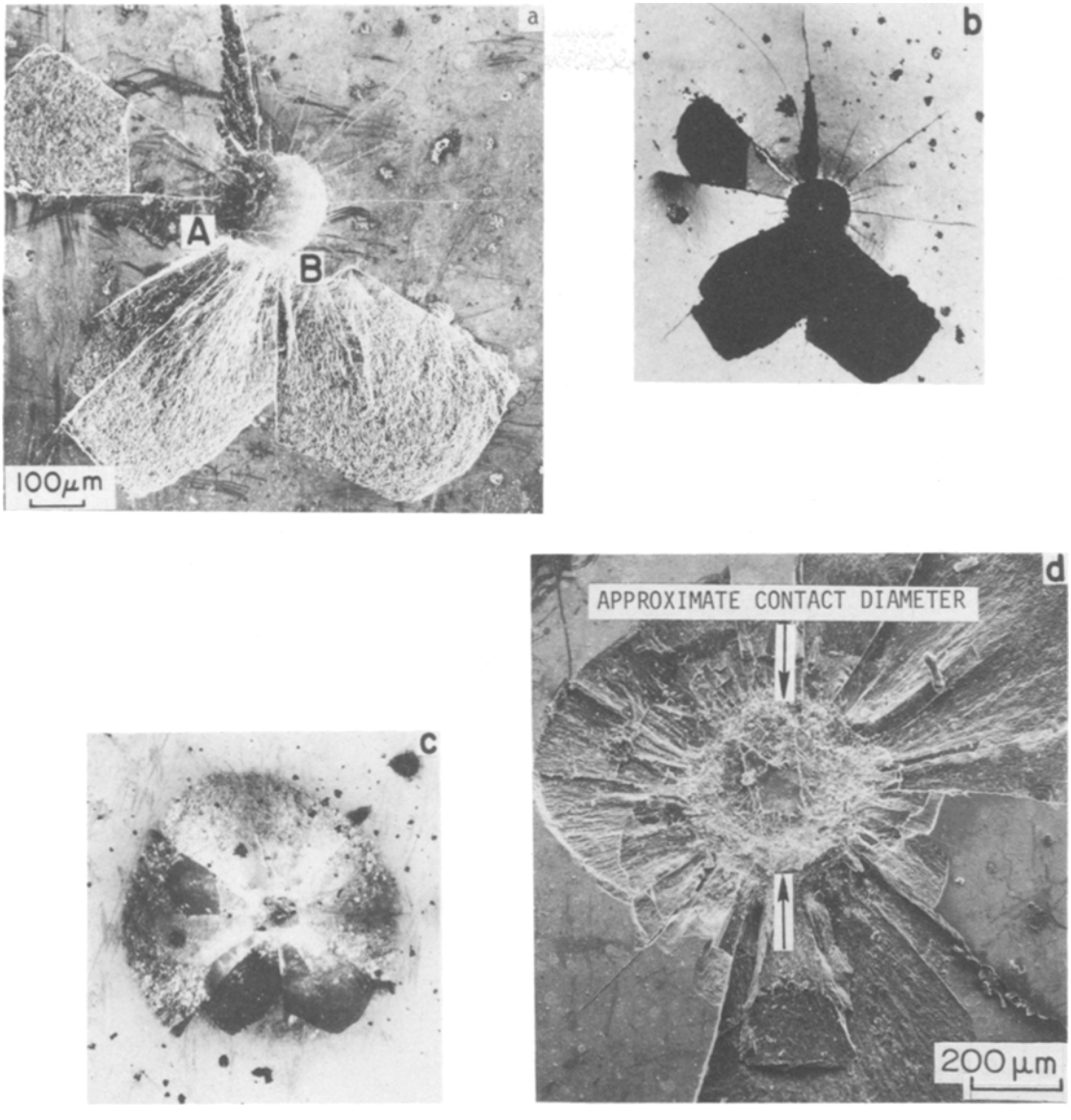

Figure 10 Micrographs of the damage caused by WC projectiles. (a) A scanning electron micrograph of the damage created by a 130 m sec^{-1} projectile, emphasizing the plastic impression and the material removal caused by lateral fracture. (b) An interference reflection optical micrograph of (a), emphasizing the radial cracks and the material pile-up around the impression. (c) A reflected polarized light micrograph of (a), emphasizing the sub-surface lateral fracture. (d) A scanning electron micrograph of the damage caused by a 520 m sec^{-1} projectile, showing the partial removal of the plastic impression.

to elastic contact. The crack length, impression radius relations for the radial and lateral cracks created by the glass projectiles are plotted in Fig. 11. There is no correlation with the fracture data obtained using the WC projectiles.

Finally, we note an interesting feature of the lateral cracks formed by both the glass and WC projectiles, namely, the occurrence of undulations near the fracture terminations (Fig. 15a); similar features are not apparent in cracks formed quasi-statically [2].

3.2. Quasi-static studies

3.2.1. Macrocrack formation stress

The elastic macrocrack formation stress can be characterized by performing elastic indentation

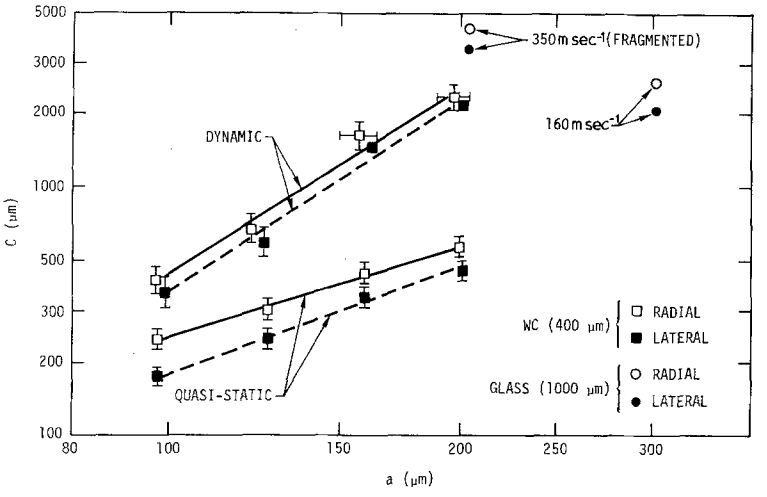

Figure 11 Radial and lateral crack lengths obtained in the dynamic tests using WC and glass projectiles, plotted as a function of the impression radius, and compared with the crack lengths obtained statistically with a 400 μm WC sphere.

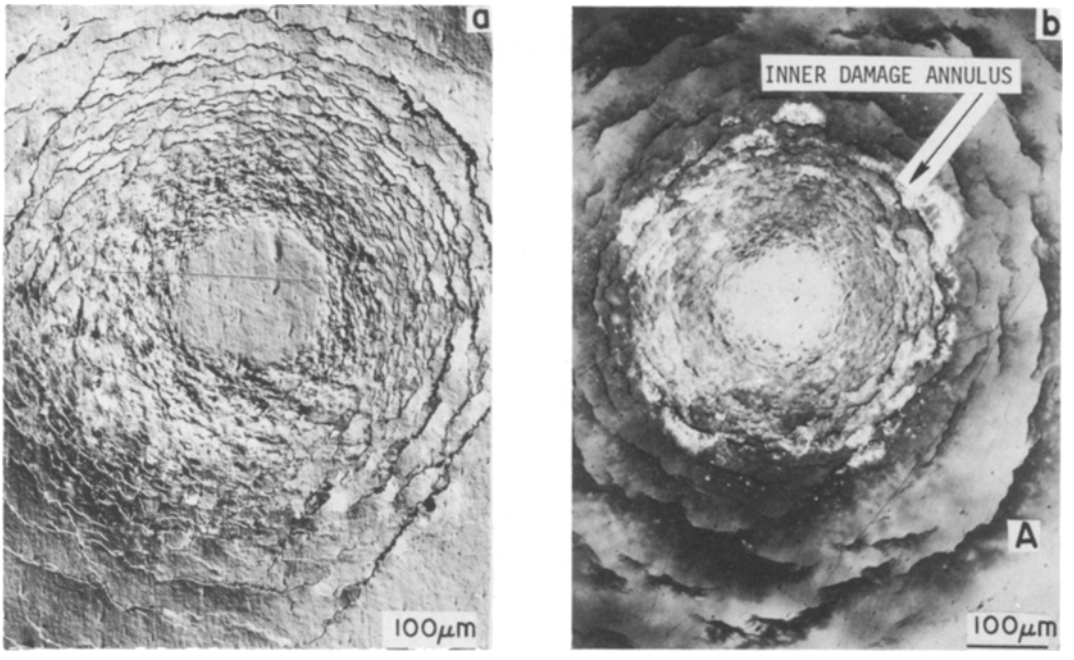

Figure 12 Micrographs of segmental ring cracks formed by nylon projectiles at 1000 m sec^{-1}. (a) Interference reflected light micrograph emphasizing the surface density of cracks, (b) reflected polarized light micrograph showing the inner annulus of sub-surface cracks parallel to the surface (arrowed). A indicates a region where three individual cracks have interacted.

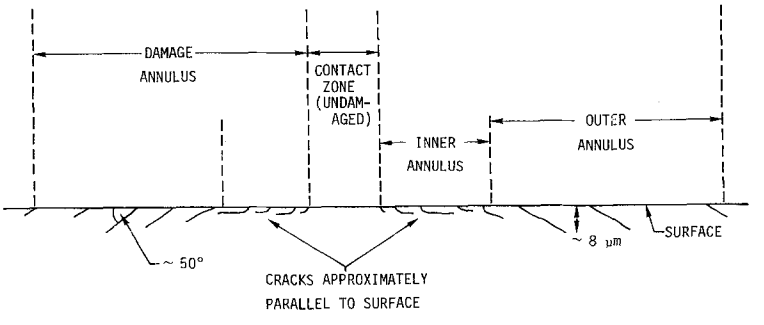

Figure 13 A schematic drawing of a section through a surface created by a fully elastic impact showing the relative crack orientations and lenghs.

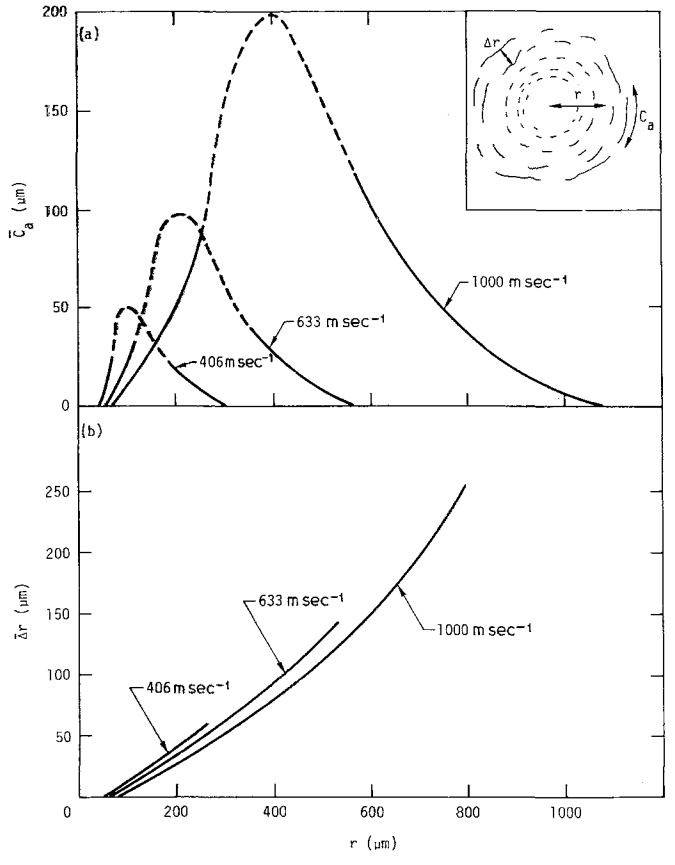

Figure 14(a) The spatial dependence of the average surface crack length, $\bar{C}_a$. (b) The spatial dependence of the average surface crack separation $\overline{\Delta r}$.

tests* (with a sphere or cylinder) to obtain the critical load, P_c, for Hertzian crack formation,† and by using the following analysis devised by Matthews *et al.* [12].

The macrocrack formation load is firstly converted into the equivalent peak tensile, σ_m, from the Hertzian relations;

$$\sigma_m = \left(\frac{1-2\nu_2}{2\pi a^2}\right) P_c$$

$$a = \left[\frac{3PR_1}{4}\left(\frac{1-\nu_1^2}{E_1} + \frac{1-\nu_2^2}{E_2}\right)\right]^{1/3} \quad (11)$$

where ν is Poisson's ratio and the subscripts 1 and 2 refer to the indenter and the sample, respectively. The cumulative probability that macrocrack formation should occur at a peak stress less than σ_m, $\Phi(\sigma_m)$, is evaluated by ordering the test data. Then for non-interacting pre-existing flaws, the flaw density function is derived from the Hertzian stress field, in terms of $\Phi(\sigma_m)$, by evaluating the product of the macrofracture probabilities in elements of size δA. The pertinent expression is [12].

$$g(\sigma_m) = -\frac{\sigma_m}{2\pi a^2} \left\{\frac{\Phi''(\sigma_m)[1-\Phi(\sigma_m)] + [\Phi'(\sigma_m)]^2}{[1-\Phi(\sigma_m)]^2}\right\} \quad (12)$$

where $g(\sigma_m)$ is the number of pre-existing flaws per unit area with a "strength" (i.e. macrocrack formation stress) in the range σ_m to $\sigma_m + d\sigma_m$. The derivation of $g(\sigma_m)$ from Equation 12 is achieved by obtaining a running computer fit to $\Phi(\sigma_m)$ using an expansion in Chebychev poly-

* Pre-existing flaw distributions can only be obtained from indentation tests if the flaws are small compared to the contact radius, as required to produce a uniform tension over the flaw length. If this condition does not pertain, Hertzian crack formation can be preceded by metastable ring fracture, and the observed macrocrack formation load does not then yield the extension condition for the pre-existing flaws.

† A convenient method for estimating P_c is to use acoustic emission as an indicator of flaw formation.

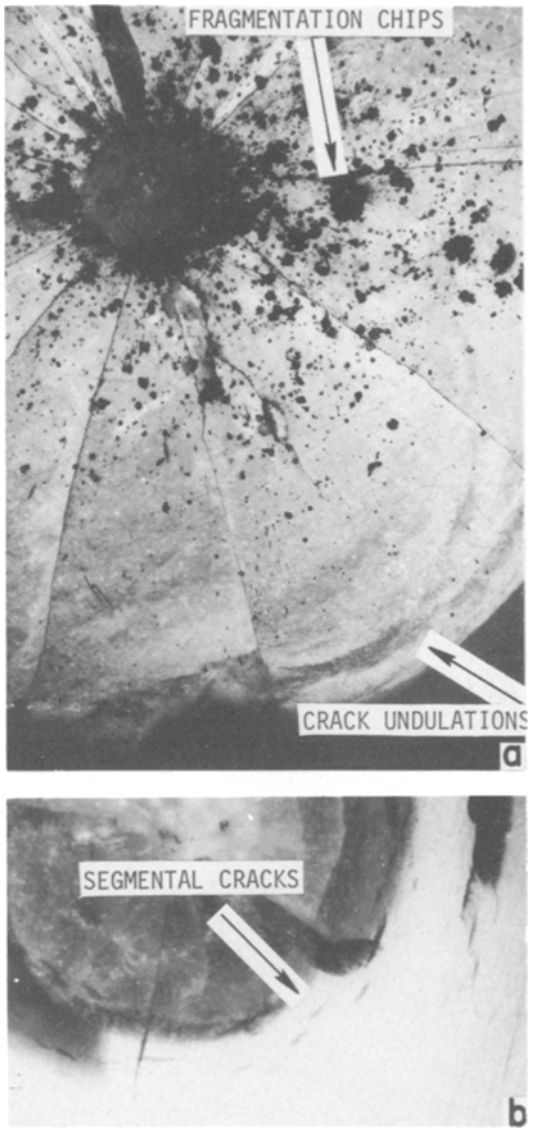

Figure 15 Reflected polarized light micrographs of the damage caused by 1000 μm glass projectiles: (a) 350 m sec^{-1}, note the fragmentation chipping around the central impression and the wavy nature of the lateral cracks (arrowed) near its arrest position; (b) 160 m sec^{-1}, note the appearance of several segmental ring cracks (arrowed) outside the main damage zone.

nomials [12] and then calculating the derivatives $\Phi'(\sigma_m)$ and $\Phi''(\sigma_m)$. Finally, the cumulative function, $G(\sigma_m)$, is derived from $g(\sigma_m)$ using

$$G(\sigma_m) = \int_0^{\sigma_m} g(\sigma_m)\, d\sigma_m \qquad (13)$$

where $G(\sigma_m)$ is the total number of flaws per unit area with a "strength" less then σ_m.

Critical macrocrack formation loads obtained for a mechanically polished ZnS sample (using soda lime glass spheres*), converted into flaw densities, $g(\sigma_m)$, are plotted in Fig. 16a. The corresponding cumulative flaw distribution function $G(\sigma_m)$ is plotted in Fig. 16b.

3.2.2. Hardness relations

Vickers hardness values for ZnS have been determined at temperatures of 30° C and −196° C and at displacement rates from 10^{-6} to 10^{-2} m sec^{-1}. The data are plotted in Fig. 17. The hardness increases with increase in displacement rate and with decrease in temperature. The data at the two temperatures tend to converge at ~ 10 m sec^{-1} to a value of ~ 3 GN m^{-2}. This displacement rate is below the particle velocity expected for most impact experiments of current interest and, being equivalent to a plastic strain-rate of 10^4 sec^{-1},† is typical of the rates needed to obtain viscous drag [6]. A value of 3 GN m^{-2} is thus assumed, hereafter, to be the quasi-static hardness that pertains to low velocity impact situations.

4. Damage analysis

4.1. Elastic response

A complete estimate of the contact parameters that pertain to the nylon impacts is not presently possible, because the nylon exhibits extensive permanent deformation, and the constitutive equations that characterize this deformation are not well formulated. A similar difficulty exists for water drop impacts [8]. An approach to damage prediction that does not require a detailed knowledge of the contact is thus required.

The short circumferential cracks observed in the elastic response regime are quite consistent with the large amplitude, short duration stress waves predicted by the dynamic elastic analysis. A quantified form of this analysis might, therefore, be capable of damage prediction, and we suggest herein, a semi-empirical approach for this purpose. The spatial dependence of the impact crack density (Fig. 12) is superimposed onto the flaw density curve (Fig. 16b) to estimate the peak surface tensile stress distribution for each impact.

* The choice of soda lime glass is an important one. The above analysis of flaw statistics only applies if the simple ($1/r^2$) Hertzian stress field pertains. Since this stress field can be substantially modified by friction [13], the indenter should be chosen to have an elastic modulus comparable to the sample, as required to minimize displacement mismatch at the interface.

† The plastic strain in hardness tests is 0.08 [14].

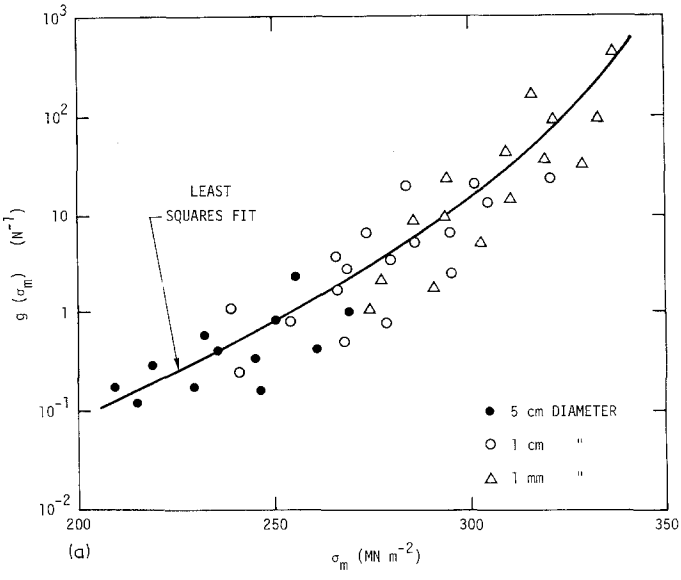

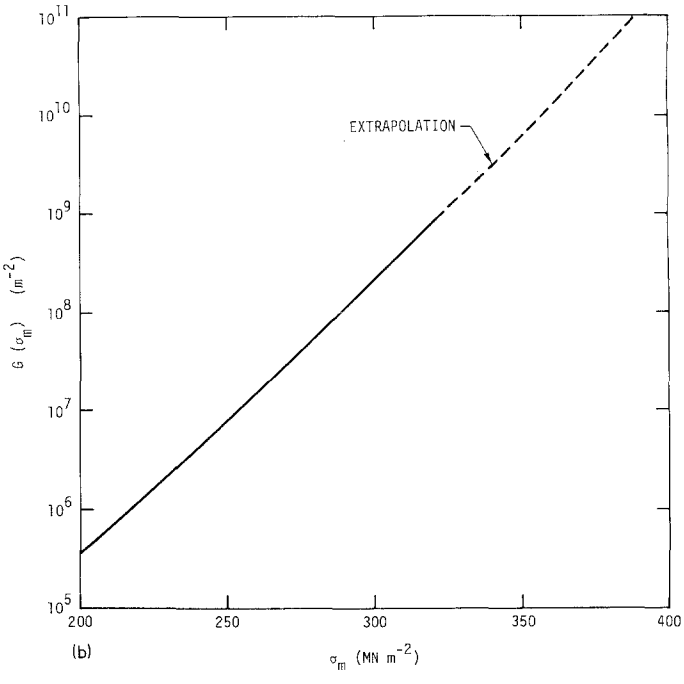

Figure 16(a) The flaw density function $g(\sigma_m)$ for ZnS obtained using glass spheres. (b) The cumulative flaw density $G(\sigma_m)$ derived from (a).

These stress distributions are then compared with the dimensional predictions of the dynamic analysis (Equation 8) to determine consistency. If consistency is obtained, the contact parameter k can be determined empirically as a function of the elastic properties of the target and the elastic/plastic properties of the projectile. Thereafter, the normalized stress fields can be constructed and the impact damage predicted by superimposing the quasi-static indentation fracture characteristics of the target.

The key issues that determine the utility of the peak surface stress evaluation are whether the ambiguity in the crack density (especially in the region of extensive crack interaction), or the failure to extend precursors into observable macrocracks (because of the short stress duration in the inner zone), lead to uncertainties in the deduced stress amplitude in critical portions of the stress field. A plot of the peak surface tensile stress, shown in Fig. 18, demonstrates that the region of extensive crack interaction (indicated by the dotted

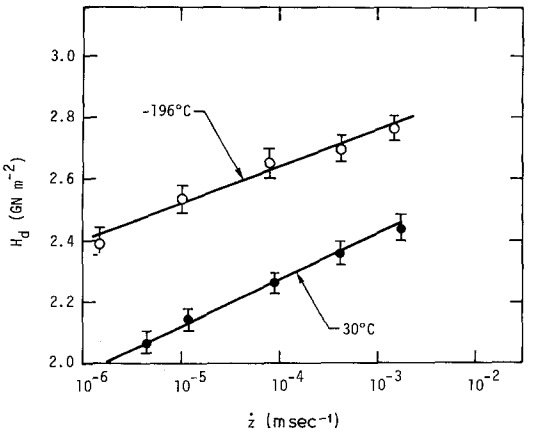

Figure 17 The rate dependence of the Vicker's hardness for ZnS at two temperatures.

portions of the curves) occurs in a non-critical position and, therefore, does not adversely affect the utility of the semi-empirical method. The effect of the stress duration on crack extension in the inner zone is less apparent. However, the occurrence of a maximum in the tensile stress curve outside the contact zone is consistent with the expectation of the stress wave analysis (Fig. 6), and the crack lengths in the vicinity of the maxima are large enough, 15 to 30 μm (cf. Figs. 18 and 14a), that the non-activation of precursors in this zone seem unlikely.

A cursory examination of the present results indicates, however, that the stresses are not consistent with the unique normalized stress field expected from the dynamic stress analysis (Equation 8), because the stress maxima do not increase as rapidly as the contact pressures. This suggests that (if the stress determinations are valid) the one-dimensional shockwave method may be providing inconsistent predictions of the contact pressure. Further evidence supporting this contention is presented later.

4.2. Plastic response*

Since the WC and glass projectiles did not experience permanent deformation during the impacts, it may be possible to predict the contact parameters by assuming an incompressible projectile.

Initially, therefore, the duration of the first pressure pulse is determined from the projectile dimensions and the shock propagation velocity, and the contact radius at the end of the pulse is

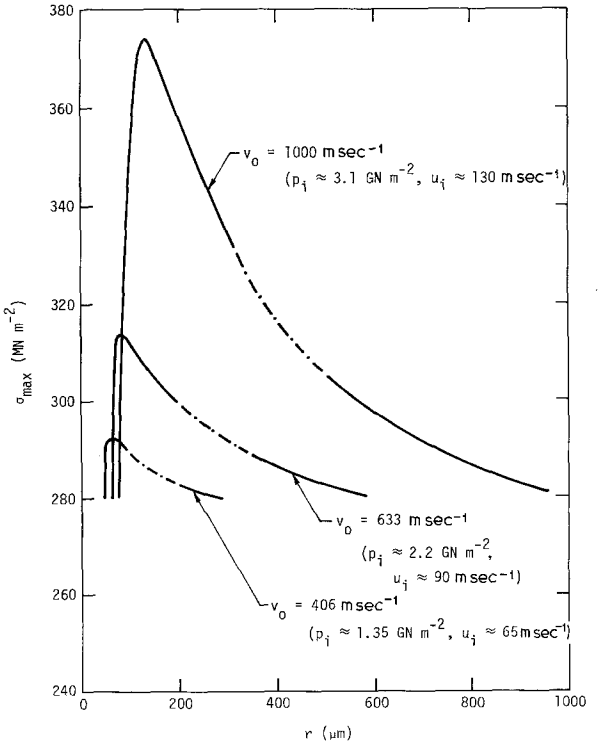

Figure 18 The spatial dependence of the peak dynamic tensile stress obtained from the measured surface crack densities; the dotted portion is the region of extensive crack interaction.

* The term "plastic" response is used to describe the response which leads to the radial, lateral and median crack formation which is typical of plastic response in quasi-static indentation. However, it cannot yet be unambiguously concluded that a plastic target response is required for this type of fracture in dynamic situations.

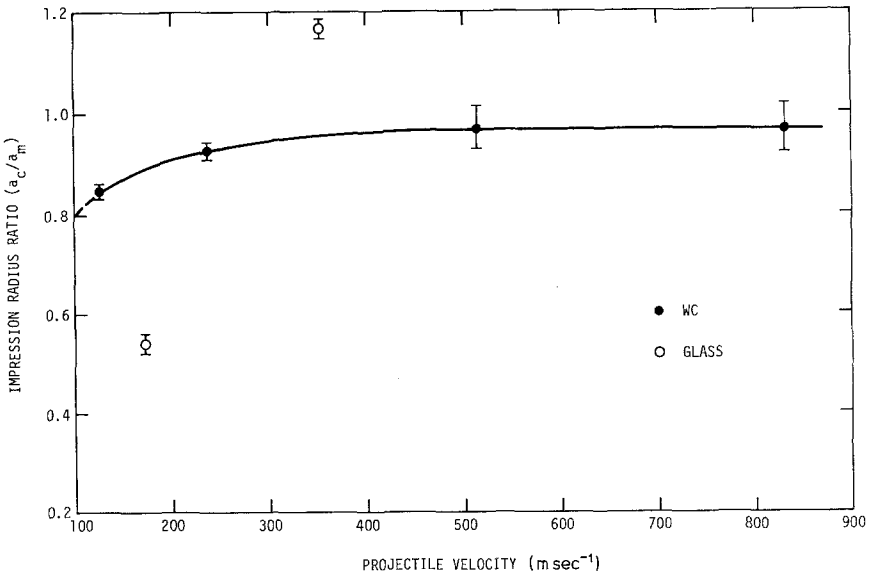

Figure 19 The ratio of the contact radius predicted from the first pressure pulse to the measured contact radius, plotted as a function of the projectile velocity.

then calculated from Equation 6. The ratio of this contact radius, a_c, to the final measured contact radius, a_m is shown in Fig. 19. The accuracy of the predictions for the WC projectiles suggests that the incompressible approximation is probably reasonable for such projectiles, and that the deformation damage, except at the lowest velocity, is largely created during the initial period of contact. (The relatively lower calculated contact radius at the lowest velocity indicates the probability of additional deformation occurring later in the contact period in this velocity range; a tendency that is likely to become more pronounced as the velocity is further decreased.) The contact radii calculated for the glass projectiles are substantially more deviant. The relatively larger value of the calculated contact radius at the higher velocity is undoubtedly a consequence of projectile fragmentation prior to the completion of the first stress wave transit, which prematurely terminated the development of the plastic impression. The low ratio obtained at the lower velocity is probably a more typical result in the absence of fragmentation, and indicates that the assumed contact behaviour is not as applicable for glass projectiles – whether this is due to the relatively higher compressibility or the lower acoustic impedance of glass (compared to WC) remains to be determined.

The resemblance of the impact damage in the plastic regime to that obtained quasi-statically [2] suggests that the quasi-static fracture characterization (Fig. 1) might also pertain to the impact fracture problem. The shock-wave contact pressure is thus combined with the calculated contact radius and the fracture toughness† to obtain a numerical value for the dimensionless indentation fracture parameter, $K_D\Phi/H_d\sqrt{a}$, at the completion of the first pressure pulse. Then, by referring to the calibration curve (Fig. 1), the normalized crack length, C/a, and hence C, can be predicted. The ratio of the predicted radial crack lengths, C_c, to the measured crack lenghts, C_m, is plotted as a function of the projectile velocity in Fig. 20. For the WC projectiles, the predicted crack lengths are in good agreement with the measured crack lengths, except at the lowest velocity. For the glass projectiles the predictions substantially underestimate the crack extension. However, we note the interesting result that if the effective acoustic impedance of the glass is assumed to be large, e.g. similar to that for WC, the predicted crack lengths approach the measured crack lengths, and a good correlation is then obtained at the higher velocity.

An equivalent quasi-static prediction of the crack lengths can be made, if the *measured* im-

† The dynamic fracture toughness, K_D, of ceramics is generally similar to the quasi-static toughness, K_c: hence, K_D is assumed herein to be equal to [2] 1 MN m$^{-3/2}$.

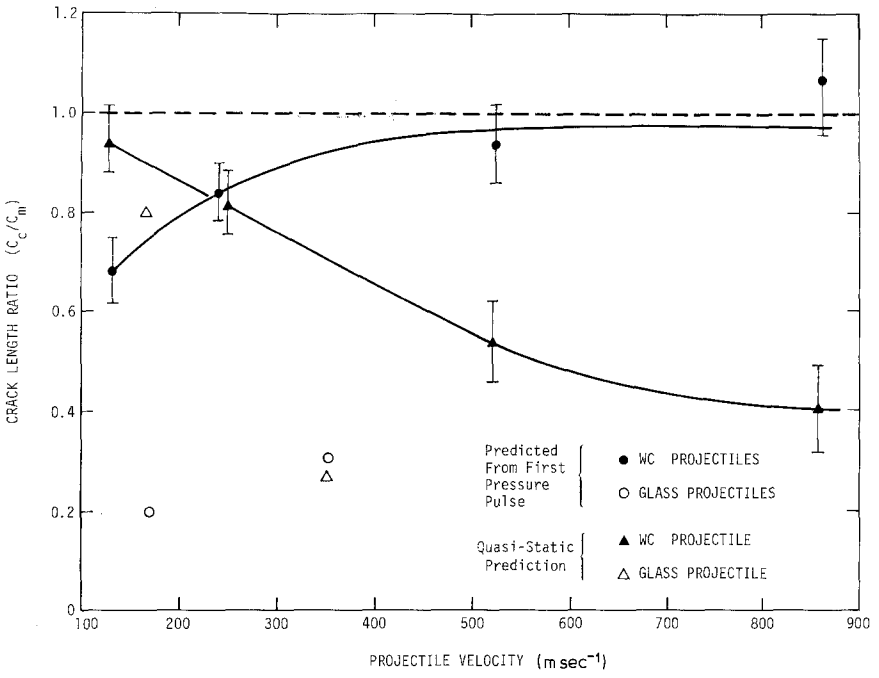

Figure 20 The ratio of the radial and lateral crack lengths, as predicted from the (first pressure pulse) dynamic analysis or the quasi-static analysis, to the measured radial and lateral crack lengths.

pression radii are combined with the athermal quasi-static hardness (3 GN m^{-2}). The crack lengths predicted by this approach are plotted in Fig. 20. The predictions are reasonably good at the lowest velocities ($\lesssim$ 160 m sec^{-1}) for both projectiles, but become more deviant as the velocity increases.

5. Discussion

The impact damage caused by a projectile has been shown to be markedly different for elastic and plastic conditions. It is thus of crucial importance that the nature of the contact – for a specified target, projectile combination – be predictable, in terms of readily measured target and projectile properties. The combination of one dimensional shock wave and quasi-static hardness data as an approach for predicting the contact behaviour seems to provide an approximate preliminary indication. However, this method is inadequate in the transition range: for example, the glass and WC projectiles at their lowest velocities (160 and 130 m sec^{-1} respectively) resulted in a plastic target response,‡ whereas the one-dimensional shock wave data indicated a contact pressure below the athermal quasi-static hardness. Conversely, the nylon at its highest velocity (1000 m sec^{-1}) produced an elastic target response, although the shock wave data indicated a pressure equal to the athermal quasi-static hardness. Similar indications of a deficiency in the one-dimensional method for predicting the contact behaviour were obtained from the peak surface stress determinations in the elastic response regime (Section 4.1). The three-dimensional aspects, or the transient nature, of the contact appear, therefore to be asserting an important influence on the contact behaviour. One such possibility suggested by the present observations is that the contact is predicated by whichever material, target or projectile, first becomes plastic; such that the other material remains elastic for an extended period thereafter. This important issue is presently being addressed by the empirical evaluation of the target response and pressure characteristics obtained with a range of different target and projectile materials, combined with a three-dimensional numerical analysis of specific particle impacts.

In the plastic response regime, the relatively good low velocity ($\lesssim$ 160 m sec^{-1}) predictions obtained using a quasi-static approach augur well for the development of an effective low velocity erosion model, along the lines suggested in an earlier paper [12]. However, the elastic/plastic

‡ There were indications, however, of an imminent transition for the glass projectile (see Section 3.1.4).

penetration aspects of the problem needs further attention before absolute predictions are possible. The varied predictability of the high velocity damage, obtained using the one-dimensional dynamic analysis of the first pressure pulse, indicates that this approach has merit,* but that its regime of applicability and its limitations need to be established. Further damage studies in the plastic response regime for a range of different target and projectile materials are being conducted for this purpose.

In the elastic response regime, the empirical determination of the dynamic tensile stress from crack patterns or dislocation motion [15] appears to be a prerequisite to damage prediction, since the contact parameters (e.g. k in Equation 8) can be inferred from such data. Thereafter, the effects of the important elastic damage parameters, E, ρ, σ_c, K_c can be systematically studied using a range of different materials and various surface treatments.

Although a considerable amount of testing and analysis is still needed to quantify the impact damage, the initial results presented in this study have suggested the following important requirements for good impact damage resistance. Firstly, since the damage in the elastic regime appears to be much less intense than that observed in the plastic regime, a target which responds elastically is preferred. When an elastic response can be achieved, a large fracture toughness and longitudinal wave velocity, and a small surface (or near surface) flaw size are expected to be the prime requirements for good damage resistance. When plastic response is inevitable, the important target properties are expected to be a large fracture toughness and a small elastic modulus, as needed to minimize the fracture extension.

6. Conclusions

(1) The impact damage observed under fully elastic contact conditions has been shown to consist of an annulus of segmental ring cracks created by near-surface transient tensile stresses.

(2) The impact damage observed under fully plastic contact conditions has been shown to be identical in form to that obtained quasi-statically, consisting of radial, lateral and median cracks outside a central plastic impression.

(3) A semi-empirical analysis of elastic impact fracture, based on the measurement of flaw densities in the damage annulus, has suggested an approach for predicting impact damage.

(4) An analysis of plastic impact fracture has shown that a quasi-static approach provides a reasonable damage prediction at low velocities ($\lesssim 160\,\mathrm{m\,sec^{-1}}$); while a dynamic approach, based on the one-dimensional pressure during the first pulse, appears to be tenable at high velocities ($\gtrsim 400\,\mathrm{m\,sec^{-1}}$).

(5) Some of the target properties expected to influence the impact damage, have been inferred from the present test results.

(6) Suggestions have been made concerning empirical and analytic studies which would further quantify our capabilities for predicting impact damage from the basic properties of the target and projectile.

Appendix. Crack arrest in dynamic stress fields

The velocity of crack in a rapid propagation event ranges from zero to a maximum value, v_T, which is a fraction of the longitudinal wave speed, c_t [16]. The average velocity, $\bar{v}$, will also be a function of c_t, and of the maximum stress intensity factor, K_m, acquired during the fracture event [17]. In general, therefore,

$$\bar{v} = \kappa(K_m)\, c_t \tag{A1}$$

where κ is a function of K_m. But, the average velocity is related to the crack arrest length by:

$$\bar{v} = \frac{C_a - C_0}{\Delta t} \tag{A2}$$

where Δt is the propagation time and C_0 is the initial crack length. Generally, $C_a \gg C_0$; hence in terms of the normalized time ΔT (Equation 6), the crack arrest length can be derived from Equations A1 and A2 as:

$$C_a \approx \frac{k^2 \kappa(K_m)}{4 c_t} \Delta T. \tag{A3}$$

In contact situations, crack arrest in brittle materials usually occurs when the stress intensity factor is approximately equal to the critical stress intensity factor, K_c [17]. Hence, for a uniform

* It is perhaps surprising that such good predictions are obtained for the WC projectiles, since there appear to be problems with the pressure predictions derived using the one-dimensional shock wave method.

tensile stress over the crack surfaces, the crack arrest stress, Ω_a, is given by [17]:

$$\Omega_a \approx \frac{K_c}{p_i\sqrt{(\pi C_a)}} \tag{A4}$$

while the crack propagation stress, Ω_c, is:

$$\Omega_c \approx \frac{K_c}{p_i\sqrt{(\pi C_0)}}. \tag{A5}$$

The crack propagation time ΔT can be derived from Equations A4 and A5 if $\Omega(T)$ in the tensile region is known. An exact analytic form for $\Omega(T)$ does not exist, but an approximate $\Omega(T)$ will permit a parametric relation for ΔT to be obtained in terms of the important impact variables. The simplest $\Omega(T)$ that exhibits some similarity to the anticipated stress variation (Fig. 5) is the sinusoidal stress;

$$\Omega = \Omega^* \sin(\pi T/T_0). \tag{A6}$$

From Equation A6, the crack propagation interval is:

$$\Delta T = \frac{T_0}{\pi}\left[1 - \sin^{-1}\left(\frac{\Omega_a}{\Omega^*}\right) - \sin^{-1}\left(\frac{\Omega_a}{\Omega^*}\right)\right]. \tag{A7}$$

Substituting for Ω_a from Equation A4 then gives:

$$\Delta T = \frac{T_0}{\pi}\left[1 - \sin^{-1}\frac{K_c}{\Omega^* p_i\sqrt{(\pi C_a)}} - \sin^{-1}\frac{\Omega_c}{\Omega^*}\right]. \tag{A8}$$

Solving Equations A3 and A8 for C_a gives the parametric result:

$$C_a \approx \frac{k^2}{4c_t}\kappa(K_m)\,\Delta T(p_i/K_c, \Omega_c^{-1}, T_0, \Omega^*). \tag{A9}$$

Acknowledgements

The authors acknowledge the financial support of the Office of Naval Research under Contract No. N00014-75-C-0669. They also wish to thank T. L. Menna for extensive assistance, especially in the performance of the single particle impact experiments, and J. C. Chessnutt for the scanning electron micrographs. Finally, we acknowledge several informative discussions with M. E. Graham and W. F. Adler.

References

1. B. R. LAWN and T. R. WILSHAW, *J. Mater. Sci.* **10** (1975) 1049.
2. A. G. EVANS and T. R. WILSHAW, *Acta Met.* **24** (1976) 939.
3. A. G. EVANS and E. A. CHARLES, *J. Amer. Ceram. Soc.* **59** (1976) 371.
4. B. R. LAWN, *Wear* **33** (1975) 369.
5. W. GOLDSMITH, "Impact" (Arnold, London, 1960).
6. P. L. STUDT, E. NIDICK, F. URIBE and A. K. MUKHERJEE, "Metallurgical Effects at High Strain Rates", edited by R. W. Rohde *et al.* (Plenum, New York, 1973) p. 379.
7. R. M. BLOWERS, *J. Inst. Maths. Applic.* **5** (1969) 167.
8. W. F. ADLER, AFML-TR-73-174 (1974).
9. G. T. HOFF, G. LANGBEIN and H. RIEGER, ASTM STP 409 (1967) p. 42.
10. M. E. GRAHAM, J. D. CARLYLE and T. L. MENNA, *Rev. Sci. Instrum* **46** (1975) 1221.
11. T. L. MENNA, M. E. GRAHAM and J. D. CARLYLE, Momentum Considerations in Particle Specimen Interactions, Effects Technology Inc., October 1975.
12. J. R. MATTHEWS, F. A. MCCLINTOCK and R. A. SHACK, *J. Amer. Ceram. Soc.* **59** (1976) 304.
13. K. L. JOHNSON, J. J. O'CONNOR and A. C. WOODWARD, *Proc. Roy. Soc.* **A334** (1973) 95.
14. D. TABOR, "Hardness of Metals" (Clarendon, Oxford, 1951).
15. K. H. JOLLIFFEE, *Phil. Trans. Roy. Soc.* **A260** (1966) 101.
16. B. R. LAWN and T. R. WILSHAW, "Fracture of Brittle Solids" (Cambridge, 1975).
17. A. G. EVANS and T. G. LANGDON, *Prog. Mat. Sci.* **21** (1976).

Received 22 April and accepted 21 May 1976.